Single-electron stripping cross sections of N_1^+ in Ne, Ar, and Kr between 35 and 140 keV

B. Hird and H. C. Suk
Physics Department, University of Ottawa, Ottawa, K1N 9B4, Canada
(Received 2 February 1976)

The single-electron stripping cross section for N_1^+ ions in targets of Ne, Ar, and Kr have been measured in the energy range 35 to 140 keV. It was found that the observation of the linear relationship between the target pressure and the counting rate is an inadequate test for single-collision conditions in these reactions. The angular spread was found to be significant, and the lack of agreement among previous measurements seems to be explainable in terms of the different ways in which the angular spread was handled. The two-state and the Firsov theories of charge-changing cross sections are unable to account for the considerable differences in the cross sections between the three targets.

INTRODUCTION

The theoretical treatment of asymmetric charge-changing cross sections has usually made one of two opposite assumptions. In the two-state theory, based on the Landau-Zener-Stuckelberg model, a specific single final state only is considered,[1] whereas in the Firsov[2] approach the transferred electron is assumed to be excited statistically into one of a large number of closely spaced states.

The two-state theory has been successful in predicting with fair reliability the projectile velocity at which the cross section passes through a maximum[3] in terms of a typical interaction distance and the energy defect for the collision. At velocities well below this maximum a simple formula has been obtained for the stripping cross section of one electron from a singly-charged ion,

$$\sigma_{12} = \frac{36(1.202)}{\pi} \frac{I}{13.6} \left(\frac{m}{M}\right)^2 \frac{E^2 e^4}{|\Delta E|^4},$$

where I is the ionization energy (in eV) of the incident ion of mass M, and m and e are the electron mass and charge. The notation for the cross sections used throughout the paper is such that the first subscript refers to the charge state of the incident ion and the second subscript refers to the charge state of the ion after the interaction which carries most of the energy and momentum. (The cross section σ_{12} would be described in the notation of Ref. 3 as $10/2\bar{1}$.) This cross section is strongly dependent on the energy defect ΔE, so that in the endothermic reactions low excitations are favored for the final states. Most of the energy defect in σ_{12} collisions therefore comes from the ionization potential of the projectile, since in this theory the transferred electron is likely to enter a state with nearly zero energy, either a low-energy state in the continuum or, if the negative ion is stable, to be bound with the (small) electron affinity. The final-state particles in σ_{12} reactions are both charged, so that there is Coulomb attraction between them at large separation distances and the energy defect at the interaction distance is less than that which is calculated from the binding energies. However, the correction for the Coulomb energy for a reasonable choice of the interaction distance is not large enough to account for more than about half the energy defect and the effective energy defect is still sufficiently large for the cross-section maximum to be predicted at several hundred keV.

At energies below 100 keV the energy dependence of the cross section is usually found to be less rapid than the E^2 dependence of the above two-state formula. However, a slight variation of the energy defect ΔE with projectile energy, due to higher-energy final states, would reduce the effective E dependence, assuming that higher-energy projectiles excite, on the average, higher-energy final states.

The opposite theoretical approach[2] considers the electron excitation as the heating of an electron gas, and an estimate is made for the probability of excitation of an electron in the projectile to an energy greater than its ionization potential. Firsov gives a formula $\sigma = \sigma_0[(E/E_0)^{0.1} - 1]^2$, where the constants $\sigma_0 = 33 \times 10^{-16}/(Z_p + Z_t)^{2/3}$ cm^2 and $E_0 = 270AI^2/(Z_p + Z_t)^{10/3}$ eV include some target dependence through the atomic number Z_t. The other constants, A the atomic mass, Z_p the atomic number, and I the ionization potential, refer to the projectile. Though no maximum is predicted by this theory, the relation gives about the correct energy dependence in the region below 100 keV. However, a survey[4] has shown that the magnitude of the experimental cross sections is often significantly smaller than the Firsov theory predicts.

We report σ_{12} cross-section measurements for N_1^+ ions on targets of Ne, Ar, and Kr in the energy range 35–140 keV. The ionization potential of N_1^+ is fairly high (29.6 eV), so that the maxima in the

cross sections are predicted by the two-state theory to occur well above these energies; on the other hand, our energies are high enough for the straight-line-trajectory approximation of both theories to be reasonably valid. Some experimental data already exist on the atomic-nitrogen ion bombardment of Ne and Ar targets in this energy range (Brackmann and Fite[5]). However, there is systematic disagreement by about 50% with the results of Pivovar *et al.*[6] above 300 keV, where the two sets of data overlap. The results of Dimitriev *et al.*[7] above 500 keV, where the cross sections are approximately independent of energy, lie somewhere between the other sets of measurements.

One particular source of experimental error is the small-angle scattering which takes place at these energies. Some attempt was made by Pivovar *et al.* to estimate the differential cross sections at 1° and 2°, while Dimitriev *et al.* confined their measurements to angles which were less than 5 mrad.

These results are the first from a series of measurements on charge-changing cross sections where particular emphasis is placed on minimizing the systematic errors which may have been present in many of the early experiments.

EXPERIMENTAL DETAILS

The apparatus used for the measurements had been primarily designed for measurements of differential cross sections, so that the direction, energy, and ion species of the incoming beam could be accurately determined, and the direction and energy of the stripped ions which were allowed to reach the detector could also be closely defined. A general schematic view of the apparatus is shown in Fig. 1. For the integrated cross-section measurements the accuracy in the definition of the input beam parameters was retained, but the direction and energy resolution of the stripped ions was intentionally broadened in a predetermined way so as to perform experimentally the angle integration and to ensure a constant detection efficiency which was free from errors due to small angular variations of the stripped-ion detection system.

The N_1^+ beam from an rf-type ion source, after being accelerated by approximately the correct voltage, was mass analyzed and accurately energy analyzed and stabilized by means of a double focusing, 90° deflection, 66-cm uniform field magnet. The object and image slits for this magnet were both set to approximately 0.05 cm width, giving a momentum resolution of $\Delta p/p = 8 \times 10^{-4}$. After passing through the deflection magnet, the beam was suitably focused by quadrupole magnets onto a collimator consisting of two vertical slits, each 0.22×2.4 mm^2, which were separated by a distance of 210 mm so that the incident direction was defined to $\pm 1.5'$ of arc in the horizontal direction. The second of these slits also acted as the entrance aperture to the differentially pumped gas target. Large holes were made in the sides of the collimator tube to ensure that the pressure within the collimator between the slits was much lower than in the gas-target region. Downstream of the gas target a horizontal exit slit of vertical width 0.06 mm was placed 63 mm from the collimator and the region beyond it was differentially pumped,

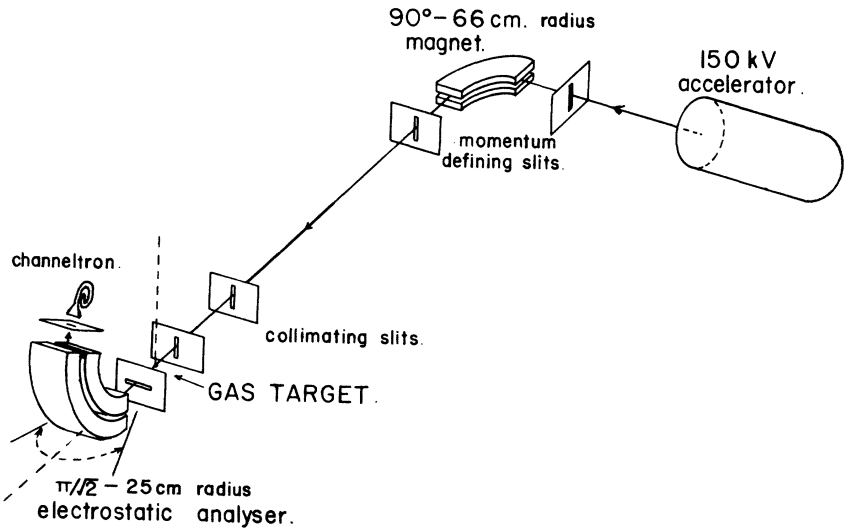

FIG. 1. Schematic diagram of the accelerator and the apparatus which accurately defines the incident and the scattered beams both in energy and direction. All beam-focusing and antiscattering devices which do not alter the beam emittance have been omitted.

so that this horizontal slit defined the downstream end of the gas target. A portion of the ions from the vertical entrance slits which traversed the target from the collimator also passed through the horizontal exit slit and entered the electrostatic analyzer, where they were deflected in an upwards direction. The horizontal exit slit also defined the object position and size for the focusing properties of the analyzer. The electrodes of this analyzer produced an accurate cylindrical field distribution in the region of the ion trajectories, with a central ray radius of curvature of 254 mm. The gap between the cylindrical electrodes was 12.5 mm, so that electrode voltages of approximately one-tenth of the accelerator voltage were required to deflect the ions to the image slit, behind which was placed a channel electron multiplier. The first-order focus of the ions occured at a deflection angle of slightly less than $\pi/\sqrt{2}$, because a small proportion, about 25 mm, of the total ion trajectory between the object and image slits was outside the electric field region.

The combined system of the accelerator, the 90° magnet, and the electrostatic analyzer was known to have an energy resolution of better then $\Delta E/E = 10^{-3}$, with long-term stability, from preliminary tests with a narrow image slit. For the present measurement the image-slit width was increased to 0.95 mm, with the result that the energy-resolution profile became flat topped, showing that no change in detection efficiency occurred for small shifts in the magnet or in the electrostatic-analyzer parameters. The second-order aberrations in the electrostatic analyzer[8] were small enough to allow all the ions which did not strike the electrodes to reach the channel multiplier, giving an angle of acceptance of ±2° in the vertical direction for ions from the gas target. The length of the collimator slits in the vertical direction was such that the incident beam was defined vertically to within ±0.7°, although only a small proportion of this possible angular range was likely to be occupied with beam. By comparing these two angles it can be seen that all vertical deflection angles in the charge-changing interaction up to at least 0.7° were accepted by the analyzer, but losses of ions beyond these deflection angles were possible.

In the horizontal plane, the electrostatic analyzer produced no focusing, the ions being deflected only in a vertical direction by the cylindrical electrode geometry. The horizontal angle of acceptance to ions from the target was therefore determined by the 7.8 mm length of the image slit and the path length through the analyzer, giving a horizontal acceptance angle of 0.76°, which was much larger than the ±1.5′ angular spread of the ions from the entrance collimator. It was possible to rotate the entire electrostatic analyzer about a vertical axis through the center point of the gas target, to an accuracy of ±10″, so as to obtain the angular profile and to permit accurate alignment of the system. With the image-slit length used in the integrated cross-section measurements the horizontal angle profile of the incident ions was found to be flat topped and of width in close agreement with the above calculations (Fig. 2). The stripped ions from the gas target were found to produce less steep counting-rate profiles than the singly charged ions, showing that deflection angles of the order of the angular resolution were produced in the stripping process. However, a central region of the profile was always found which was reasonably flat, and the ratio of the stripped-ion to the unstripped-ion counting rates was always taken in the central plateau regions of the respective energy and angle profiles. A correction was made afterwards for the small proportion of stripped ions which were generated at angles greater than ±0.7°, both horizontally and vertically.

The target pressure was measured with a capacitance manometer[9] which was connected through a short length of $\frac{1}{4}$-in. pipe to the gas target in a region well away from the gas flow through the

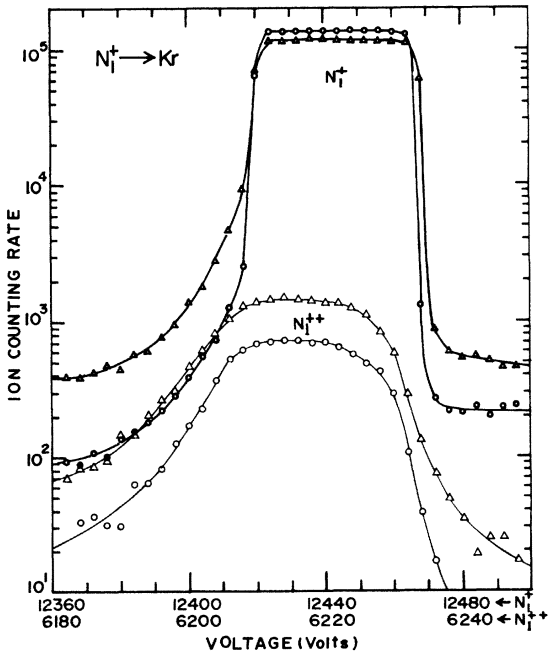

FIG. 2. Energy profile of the incident N_1^+ ions and of the charge-changed N_1^{++} ions obtained by variation of the electrostatic analyzer voltage. The incident ions had an energy of 124.9 keV. Circles: Obtained with a target pressure of 1.8×10^{-4} Torr. Triangles: Obtained with a target pressure of 9.8×10^{-4} Torr.

slits. In spite of being thermostatically controlled by a proportional heater circuit, the gauge was found to be sensitive to short-term ambient temperature variations. The stability was much improved by enclosing the gauge within a polystyrene-foam-lined box, after which drifts were reduced to less than 10^{-5} Torr per day.

The target-gas pressure was controlled by a thermal-mechanical leak in the range between 10^{-4} and 10^{-3} Torr. Care was taken to maintain a constant temperature at all surfaces of the target chamber which were in contact with the target gas and to allow the pressure to stabilize after each change in the thermal-mechanical-leak setting.

The normalization of the channel multiplier counting rates was made in terms of the integrated beam current which traversed the target and which struck the upper and lower parts of the entrance slit of the electrostatic analyzer. This current was typically about 10^{-13} A; it was multiplied to about 10^{-6} A in an electronic picoammeter[10] and then fed into an accurate current integrator. Since only the ratio of charges collected in consecutive measurements was required, no attempt was made to determine the absolute charge collected by the slit and neither secondary-emission suppression nor gas-pressure corrections were made. The counting rate in the channel multiplier was always kept below 6 kHz so as to minimize rate losses. The dead time of the system, as measured in a separate test, was 2.5 μsec, so that the loss corrections represented a small, although not well determined, effect because of short-term beam intensity fluctuations. The ion-counting efficiency of the channel multiplier was found to be uniform across the entrance aperture. With the discriminator level set to just above the system noise, there was no indication of counting losses[11] from the region of decreased multiplier gain where the ions entered the channel directly. It was found necessary to place a positive potential on the image slit just in front of the grounded multiplier cone in order to suppress secondary electrons which were emitted from the electrostatic analyzer electrodes and which otherwise generated satelite peaks in the ion-energy profile. With a positive slit bias of 70 V the satelites were reduced to less than 10^{-3} of the main peak intensity. The effective counting aperture was found to be unchanged by the slit bias.

EXPERIMENTAL PROCEDURE

The cross section σ_{12} for the stripping of atomic nitrogen is defined experimentally by the relation

$$N^{++} = N^{+}\sigma_{12}Ln \qquad (1)$$

under single-collision conditions. Here, we define N^+ as the number of ions of the initial charge state which traverse the target, and N^{++} as the number of ions of the final charge state which are created in the target whose effective length is L and atomic density is n. In experimental measurements the variation of the ratio N^{++}/N^+ is obtained over a range of n values which are produced by varying the target-gas pressure. A linear relation between the counting ratio and the target-gas pressure is conventionally used as evidence of the validity of this formula and therefore of single-collision conditions.

The numbers of counts in the channel multiplier at the image of the electrostatic analyzer may be used to obtain the ratio N^{++}/N^+, but these counts do not directly represent the number of ions which traverse the target, since a good fraction of the ions was lost by striking the exit slits. However, if the fraction lost was the same for the N^{++} ions as for the N^+ ions, the ratio of these counting rates would correctly give the ratio N^{++}/N^+. It was therefore important to ensure that the geometry of the beam and target conditions remain the same between the measurements of the two different charged states and that the increased angular spread in the N^{++} ions be accurately taken into account.

The effects of the angular spread in the stripping process may be included by interpreting N^{++} and N^+ as being proportional to the areas under the angle and energy profiles of the electrostatic analyzer, rather than just as the ratio of the optimized counting rates. The procedure followed for each cross-section measurement was as follows: At the lowest gas pressure, that is, with no gas flow to the target but with the target region pumped only through the slits, the energy and angle counting-rate profiles of the incident and stripped ions were first measured. The energy profile $N(V, \overline{\theta})$ was obtained by plotting the ion counting rate against the deflection voltage V on the analyzer electrodes, and the angle profile $N(\theta, \overline{V})$ was obtained by mechanical rotation of the analyzer abount the center point of the target. Figure 2 shows an example of the energy profiles $N^+(V, \overline{\theta})$ and $N^{++}(V, \overline{\theta})$ obtained by changing the analyzer voltage in 2-V steps across the peaks. Figure 3 shows an example of the angle profiles $N^+(\theta, \overline{V})$ and $N^{++}(\theta, \overline{V})$ at the lowest energy of the measurements. Here the angular position of the analyzer was changed in 3′ steps with respect to the incident-beam direction. At higher energies the angular spread of the stripped ions and therefore the small-angle correction was either about the same or smaller. From these measurements the optimum angle $\overline{\theta}$ and the optimum voltages $\overline{V}^{++}$ and $\overline{V}^{+}$ were read off in the

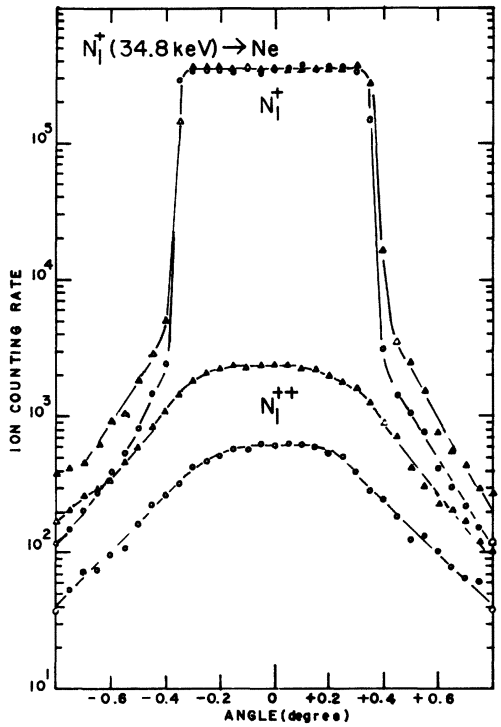

FIG. 3. Angle profile of the incident N_1^+ ions and of the charge-changed N_1^{++} ions obtained by mechanical rotation of the electrostatic analyzer about the center of the gas target. Circles: Obtained with a target pressure of 2.2×10^{-4} Torr. Triangles: Obtained with a target pressure of 8.3×10^{-4} Torr.

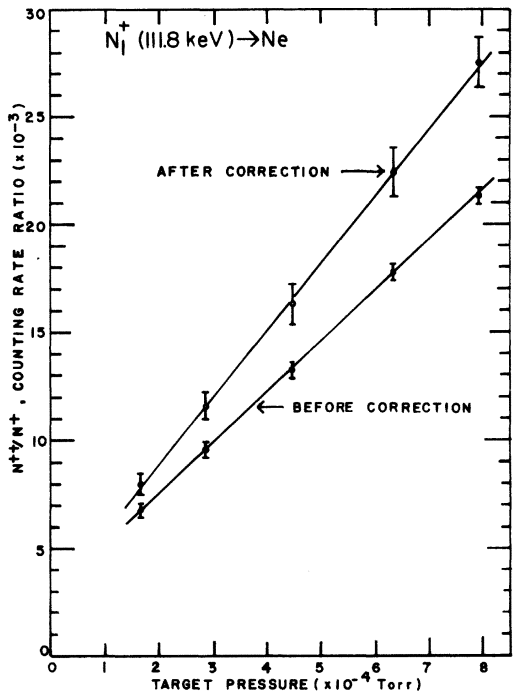

FIG. 4. Ratio of charge-changed N_1^{++} ions to N_1^+ ions which passed through the gas target, plotted as a function of the target pressure. The ratio after correction for target thickness effects is given by Eq. (6), in which the σ_1, σ_{01}, and σ_2 cross-section values are given in Table II.

central plateau regions of the respective profiles. Slight errors in the electrostatic analyzer power-supply linearity account for the few volts difference between $2\overline{V}^{++}$ and $\overline{V}^{+}$, but $\overline{\theta}$ was always found to be the same for both types of ion. The pressure variation of the ratio of counts at the optimized angle and voltages, $N(\overline{V}^{++},\overline{\theta})/N(\overline{V}^{+},\overline{\theta})$, was then determined by measuring this ratio first at the lowest, and then for successively increased, gas-target pressures. In order to minimize the effects of drift, the two counting rates were measured alternately in many short runs under stable conditions, and the totals of the counts of each type of ion were used in the ratio calculation. Figure 4 illustrates a typical variation with the target pressure of the ratio N^{++}/N^{+}, as obtained with the above procedure.

When the counting-rate ratio had been obtained over a range of pressures, the energy and angle-profile measurements $N(V,\overline{\theta})$ and $N(\theta,\overline{V})$, which had been measured at the lowest pressure, were remeasured at the highest pressure.

In order to correct the counting-rate ratio so that it represented the ratio of the areas under the energy and angle profiles, the optimized angle and energy ratio was multiplied by the correction factor

$$\frac{N(\overline{\theta},\overline{V}^{+})/\int N(\theta,\overline{V}^{+})\,d\theta}{N(\overline{\theta},\overline{V}^{++})/\int N(\theta,\overline{V}^{++})\,d\theta} \tag{2}$$

for the angle profile and by a similar factor for the energy profiles. With no change in angle or energy during the stripping process both correction factors would be unity, and the values slightly above unity which were found experimentally when the electrostatic analyzer was set at its optimized configuration $(\overline{\theta},\overline{V})$ represent the loss of stripped particles by scattering beyond the acceptance solid angle. The correction factors were found to be sufficiently close to unity, so that a linear interpolation could be made from the extreme pressures at which the profiles were obtained to the intermediate pressures at which the counting-rate ratios were measured.

The errors on the counting-rate measurements fall into two distinct groups. For one group the numbers of counts were large, so that the fluctuations from one run to the next were mainly caused by electronic drifts and changes in the beam conditions. For these the estimate for the error in the summed total of many short runs was obtained

from the fluctuations among the individual short runs. The other type of error occurred where the number of counts was small, for example, the N^{++} counts at low pressure, and here the statistical fluctuations in the number of counts dominated the error. The slope of the graph of the counting-rate ratio as a function of target pressure was obtained using a weighted least-squares fitting procedure. No estimate for the error of the target-pressure gauge was included.

TARGET THICKNESS CORRECTIONS

The pressure and target length used in the measurements were such that a few percent of the ions made more than one collision during their passage through the target gas. The exact equations which determine the relative populations of the various charge states as a function of the distance x through the target gas, neglecting interactions where the charge state changes by more than 1 in a single collision, are

$$\frac{1}{n}\frac{dN^+}{dx} = \sum_{m\neq 1}\sigma_{m1}N^{m+} - \sum_{m\neq 1}\sigma_{1m}N^+$$

and (3)

$$\frac{1}{n}\frac{dN^{++}}{dx} = \sum_{m\neq 2}\sigma_{m2}N^{m+} - \sum_{m\neq 2}\sigma_{2m}N^{++},$$

where n is the atomic density of the target gas.

In general the electron pickup cross sections are larger than the stripping cross sections by a factor between 10 and 100, so that the terms which involve stripping will be small. The N^{++} population is also much less than the N^+ population, so that many terms in these equations can be neglected. In particular, N^{3+} and higher charge states have negligible populations. With these approximations the equations become

$$\frac{1}{n}\frac{dN^0}{dx} = -\sigma_{01}N^0 + \sigma_{10}N^+,$$

$$\frac{1}{n}\frac{dN^+}{dx} = \sigma_{01}N^0 - (\sigma_{12}+\sigma_1)N^+ + \sigma_{21}N^{++}, \quad (4)$$

$$\frac{1}{n}\frac{dN^{++}}{dx} = \sigma_{12}N^+ - \sigma_2 N^{++},$$

where

$$\sigma_1 = \sigma_{10} + \sum_{m=3}^{\infty}\sigma_{1m} \simeq \sigma_{10},$$

$$\sigma_2 = \sigma_{21} + \sum_{m=3}^{\infty}\sigma_{2m} \simeq \sigma_{21}.$$

The integration of these equations is difficult, but it is possible to obtain a solution as a power series in nL, where L is the length of the target,

$$\sigma_{12} = \frac{N^{++}}{(N^+ + \frac{1}{2}N^{++})nL}\{1 - \tfrac{1}{2}(\sigma_1 - \sigma_2)nL + \tfrac{1}{12}[(\sigma_{12}+\sigma_1-\sigma_2)^2 + 4\sigma_{12}\sigma_{21} + 4\sigma_{01}\sigma_{10}]^2 n^2L^2\}. \quad (5)$$

In this expression N^{++} and N^+ refer to the populations at the end of the effective length of the target, so they have the same meaning as before. The first term in the equation can therefore be obtained from the experimental ratio N^{++}/N^+, which is the ratio of counts in the electrostatic analyzer for a given beam charge through the target. The cross section σ_{12} has been eliminated from the first-order correction term, but still remains in the second-order term. However, it is a much smaller cross section than the others in this term, and the term itself is a small correction, so that σ_{12} can safely be neglected, and the term becomes

$$\tfrac{1}{12}[(\sigma_1-\sigma_2)^2 + 4\sigma_{01}\sigma_{10}]n^2L^2.$$

The first-order correction term reached values as high as 15% for the highest pressures used in the gas target, about 8×10^{-4} Torr, and the second-order term was then about 3%, suggesting that the still higher corrections for multiple collisions in the target will be proportionately smaller and that they can be safely neglected. Figure 4 shows a typical pressure-variation graph with and without the target thickness corrections. In one curve the ratio N^{++}/N^+ is plotted against pressure, whereas in the other curve the corrected ratio

$$\frac{N^{++}}{N^+ + \frac{1}{2}N^{++}}\{1 - \tfrac{1}{2}(\sigma_1-\sigma_2)nL + \tfrac{1}{12}[(\sigma_1-\sigma_2)^2 + 4\sigma_{01}\sigma_{10}]n^2L^2\} \quad (6)$$

is plotted. The slope of these curves is then $\sigma_{12}L$ in the appropriate units. Perhaps the important conclusion, apart from the obvious change in the slope and therefore of the deduced value of σ_{12}, is that both graphs are approximately linear within experimental error, showing that the usual method of verifying single-collision conditions by checking for linearity in the uncorrected data and by making sure that $N^{++} \ll N^+$ is insufficiently sensitive and that large errors can nevertheless occur if some of the other collision cross sections are large.

The effective length of the target, L, was taken to be the physical length 63 mm between the slits. It has been suggested[12] that an end correction of twice the slit width be added at each end of the tar-

get. However, kinetic theory[13] under molecular-flow conditions predicts a gas-density distribution such that the density in the plane of the slit is the average of the internal and the external gas densites. For negligible external pressures the density at the slit is therefore half of the density far inside the target. The kinetic theory also predicts the gas-density variation on either side of the slit, and for a wide range of thin-slit shapes it predicts that there is a symmetry in the density as a function of the distance x from the plane of the slit, such that $\rho(x)=\rho_0-\rho(-x)$, where ρ_0 is the density difference from far inside to far outside the target. With such a symmetry it is easy to show that the effective length of the target for ions which traverse the entry and the exit slits is the same as the physical length and that there is no length correction due to the slit sizes, when the density inside reaches a reasonably uniform value.

The length of beam line, about 6 m, between the analyzing magnet and the gas target was kept at a pressure of about 2×10^{-7} Torr. The thickness of residual gas through which the ions passed before reaching the target was therefore about a factor of 10 less than that inside the 63-mm-length target when operated at its lowest pressures, near 2×10^{-4} Torr, so that although some charge change occurred before the ions reached the target, mainly to create N_1^0, it is a small end effect and does not invalidate the analysis.

The presence of N_2^{++} ions in the beam, which contribute to the N_1^+ counting rate but not to the N_1^{++} rate, was detected by measuring the N_2^+ ion rate, which is produced by N_2^{++} electron pickup and appears at twice the analyzer voltage. A rate about half of the N_1^{++} counting rate was found. The molecular pickup σ_{21} cross section is presumably much larger than the atomic stripping cross section, so that N_2^{++} ion contamination of the N_1^+ beam was concluded to be negligible.

RESULTS

$N_1^+ \rightarrow Ne$

The σ_{12} cross-section data, as a function of the nitrogen-beam energy, are shown in Fig. 5 and listed in Table I. It was possible to calculate the correction factor for this reaction because data are available on the cross sections σ_{10} and σ_{01} (Ref. 5) and on σ_{21} (Ref. 14) in our energy range. The correction factor input data for this reaction and for the other target gases are listed in Table II. With these values the correction is positive and increases with the beam energy, so that it reaches a maximum value of 13% at the highest energy measured. The angular and energy-spread corrections were of the same order of magnitude

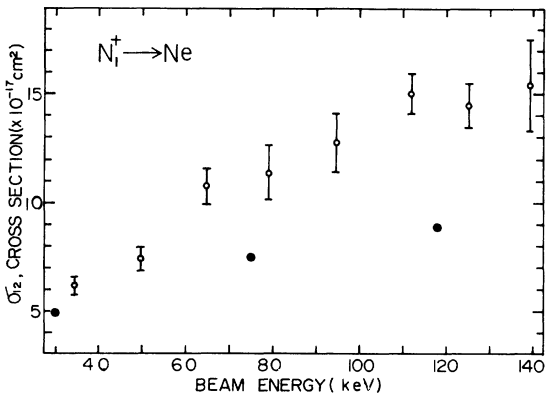

FIG. 5. Single-electron stripping cross section for N_1^+ ions in neon. Solid circles, data of Lo and Fite (Ref. 15).

for this reaction at the lowest energy and decreased to about 4% at the highest. Previous measurements[5] are also shown in Fig. 5, where we have taken the points from the graphs in the review article by Lo and Fite[15] because they are slightly more detailed than in the original paper. It appears that our values are slightly higher at the low energies, but they considerably exceed theirs at the highest energies. Our data provide a better extrapolation to the values of Pivovar *et al.*[6] at 300 keV and higher energies.

$N_1^+ \rightarrow Ar$

Figure 6 and Table I show the cross section for stripping in the argon target as a function of the beam energy. The target thickness correction, made using the published σ_{10} and σ_{01} (Ref. 5) and σ_{21} (Ref. 14) cross sections, changes sign at about 80 keV, because σ_{10} is here much larger than in the $N^+ \rightarrow Ne$ reaction, so that it exceeds the σ_{21} cross section at the lower energies, although it still is smaller than σ_{21} at the highest energies measured. The angular and energy-spread corrections were about 13% at all energies. The only previous data, those of Brackmann and Fite,[5] are also shown in Fig. 6. There is some suggestion that the energy at which the target thickness correction passes through zero is also the energy at which our data would provide an interpolation between their values. The same sort of discrepancy with Pivovar's data is again resolved when our data are extrapolated to higher energies.

$N_1^+ \rightarrow Kr$

No other measurements exist with which to compare our data on stripping in a krypton target, nor are there any data on the cross sections σ_{10} or σ_{21} which are required to make the target thickness

TABLE I. Single-electron stripping cross sections σ_{12}.

$N_1^+ \rightarrow$Ne		$N_1^+ \rightarrow$Ar		$N_1^+ \rightarrow$Kr	
Energy (keV)	σ_{12} (10^{-17} cm^2)	Energy (keV)	σ_{12} (10^{-17} cm^2)	Energy (keV)	σ_{12} (10^{-17} cm^2)
34.8	6.17 ± 0.58	34.9	1.33 ± 0.28	32.9	0.89 ± 0.32
50.0	7.42 ± 0.56	50.0	2.70 ± 0.42	49.0	1.89 ± 0.34
64.9	10.83 ± 0.85	64.5	3.12 ± 0.47	66.8	2.43 ± 0.31
79.4	11.40 ± 1.20	82.2	5.73 ± 1.08	79.4	2.74 ± 0.46
94.8	12.80 ± 1.36	96.6	6.92 ± 0.97	96.7	3.49 ± 0.51
111.8	14.96 ± 0.88	110.0	8.82 ± 0.79	111.8	4.33 ± 0.58
125.2	14.53 ± 1.04	127.0	9.53 ± 0.60	124.9	5.40 ± 0.54
139.2	15.47 ± 2.17	139.9	10.70 ± 0.87	139.9	5.78 ± 0.48

corrections. We have therefore ignored such corrections in the data shown in Fig. 7 and in Table II. This correction amounts to approximately $[10^{15}(\sigma_{10} - \sigma_{21})]\%$ (where $\sigma_{10} - \sigma_{21}$ is given in cm^2) over most of the energy range. The angle and energy-spread correction factors differed from unity by about 10% throughout the energy range, with little sign of a decrease at the higher energies.

DISCUSSION

The monotonic rise in the cross sections with energy is confirmed for all three reactions. The slight inflection which is seen in the Ne-target data at the highest energies is not statistically significant. The $N_1^+ \rightarrow$Ne collision cross section, which is much larger than the other two at the lowest energies, increases only 2.5 times through our energy range, whereas the other two cross sections increase proportionately by more than twice this ratio, in agreement with the higher-energy data of Pivovar *et al.*, who obtained the same cross section for all three targets at about 300 keV, where the $N_1^+ \rightarrow$Ne cross section seems to reach an approximately constant value. Such energies are beyond the region of validity of the near-adiabatic criterion, but there may be qualitative significance in the relative predictions of this theory. The energy of the maximum in the cross section is predicted at 260 keV for the Ne target, while it is at 360 keV for Ar and at a still higher energy for the Kr target.

The Firsov theory,[2] though it gives the general trend in the energy dependence of the cross sections quite well, has little success in its predictions of their magnitudes, both relatively and absolutely. The Ne target predictions are too large by a factor of 3, for the Ar target the factor is about 9, and predictions are 20 times too large for the Kr target. The relative ordering for the Firsov cross sections is therefore inverted compared to the experimental data.

The two-state low-energy theory makes no reference to the target, since all such information is absorbed in the drastic assumptions which have been made about the size and range of the perturb-

TABLE II. Published electron pickup and stripping cross sections which were used to make the target thickness corrections. The values of σ_{10} and σ_{01} were obtained from the graphical data of Brackmann and Fite (Ref. 5), using the review article of Lo and Fite (Ref. 15), where the graphs contain slightly more detail. The values of σ_{21} were obtained from the graphs of Fedorenko (Ref. 14).

	$N_1^+ \rightarrow$Ne			$N_1^+ \rightarrow$Ar		
Energy (keV)	σ_{01}	σ_{10} (10^{-15} cm^2)	σ_{21}	σ_{01}	σ_{10} (10^{-15} cm^2)	σ_{21}
34.8	0.31	0.24	1.8	0.31	1.5	1.1
49.7	0.32	0.35	1.8	0.33	1.4	1.2
65.0	0.34	0.40	1.8	0.36	1.3	1.2
79.4	0.38	0.43	1.8	0.39	1.2	1.2
94.8	0.40	0.43	1.8	0.42	1.2	1.2
111.8	0.41	0.43	1.8	0.44	1.1	1.2
125.2	0.42	0.43	1.8	0.46	1.0	1.2
139.2	0.43	0.43	1.8	0.48	0.9	1.2

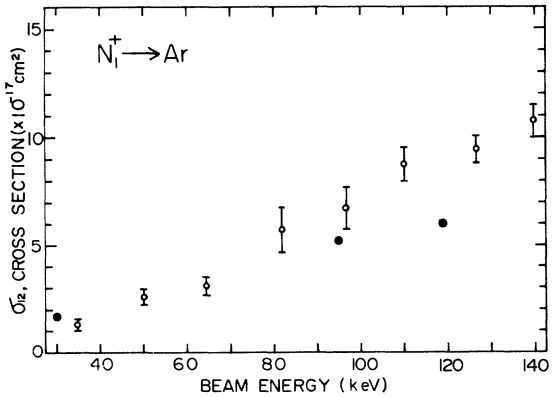

FIG. 6. Single-electron stripping cross section for N_1^+ ions in argon. Solid circles, data of Brackmann and Fite (Ref. 5).

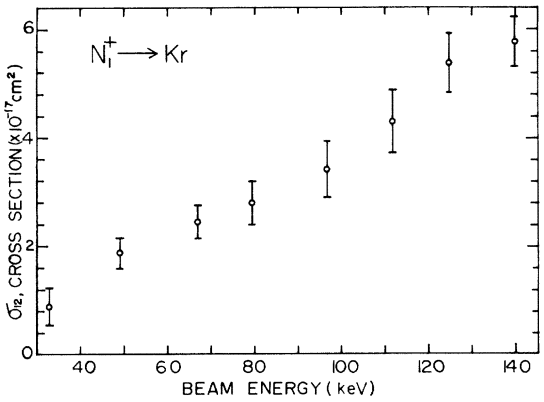

FIG. 7. Single-electron stripping cross section for N_1^+ ions in krypton.

ing interactions which cause the transition. The single-electron stripping cross sections which this theory provides for all three targets have about the correct magnitude in our energy range, but the theory's E^2 dependence does not fit the energy dependence of any of the experimental cross sections.

There is some qualitative indication from our angle-correction factors that the mean scattering angle for σ_{12} in the N_1^+ reaction decreases more rapidly with increasing beam energy than in either the $N_1^+ \rightarrow Ar$ or the $N_1^+ \rightarrow Kr$ reaction.

The considerable discrepancies which are found in the experimental data of different groups correlate to some extent with the different ways in which the angular spread in the stripped ions was handled. This angular spread is significant even at our highest energies, where several percent of the ions are scattered at angles greater than 0.7°. The other main source of error in previous data may be in the failure of the single-collision approximation, when cross sections much larger than the one being measured may significantly change the charge-state composition of the incident beam as it passes through the target even though relatively few ions result from the charge-changing cross section which is being measured.

[1]D. Rapp and W. E. Francis, J. Chem. Phys. 37, 2631 (1962); E. F. Gurnee and J. L. Magee, *ibid.* 26, 1237 (1957); A. R. Lee and J. B. Hasted, Proc. Phys. Soc. Lond. 85, 673 (1975).

[2]O. B. Firsov, Zh. Eksp. Teor. Fiz. 36, 1517 (1959) [Sov. Phys.-JETP 9, 1076 (1959)].

[3]J. B. Hasted and A. R. Lee, Proc. Phys. Soc. Lond. 79, 702 (1962).

[4]H. H. Fleischmann, R. C. Dehmel, and S. K. Lee, Phys. Rev. A 5, 1784 (1972).

[5]R. T. Brackmann and W. L. Fite, Report No. AFWL-TR-68-96, 1968 (unpublished).

[6]L. I. Pivovar, M. T. Novikov, and A. S. Dolgov, Zh. Eksp. Teor. Fiz. 50, 537 (1966) [Sov. Phys.-JETP 23, 357 (1966)].

[7]I. S. Dimitriev, V. S. Nikolaev, L. N. Fateeva, and Ya. A. Teplova, Zh. Eksp. Teor. Fiz. 42, 16 (1962) [Sov. Phys.-JETP 15, 11 (1962)].

[8]A. L. Hughes and V. Rojansky, Phys. Rev. 34, 284 (1929).

[9]Type 145BHS-1, manufactured by MKS Instruments.

[10]Type 410A, manufactured by Keithley Instruments, Inc.

[11]B. Hird, H. C. Suk, and A. Guilbaud, Rev. Sci. Instrum. 47, 138 (1976).

[12]L. H. Tokuren, M. Y. Nakai, and R. A. Langley, ORNL Report No. ORNL-TM-1988, 1969 (unpublished).

[13]G. N. Patterson, *Introduction to the Kinetic Theory of Gas Flows* (Toronto U. P., Toronto, 1971).

[14]N. V. Fedorenko, Zh. Tekh. Fiz. 24, 769 (1954).

[15]H. H. Lo and W. L. Fite, At. Data 1, 305 (1970).